Optik 125 (2014) 876–882

Contents lists available at ScienceDirect

Optik

journal homepage: www.elsevier.de/ijleo

Large field of view MEMS-based confocal laser scanning microscope for fluorescence imaging

Christin Bechtel[a,*], Jens Knobbe[b,1], Heinrich Grüger[b,2], Hubert Lakner[b,3]

[a] Institute for Semiconductor and Microsystems Technology, Technische Universität Dresden, 01062 Dresden, Germany
[b] Fraunhofer IPMS, Maria-Reiche-Street 2, 01109 Dresden, Germany

ARTICLE INFO

Article history:
Received 20 March 2013
Accepted 21 July 2013

Keywords:
Laser scanning
Confocal microscopy
Fluorescence
Optical system design
MEMS

ABSTRACT

Although confocal fluorescence microscopes are widely used in biology and have been proven to be promising diagnostic tools in dermatologic diagnostics, they are at present uncommon in medical practice. This is mainly due to high costs of acquisition and their large and complex outline. With the integration of a MEMS scanner we present a demonstration system of a confocal fluorescence laser scanning microscope which is affordable and portable. It has a field of view of 500 μm × 500 μm and is mainly composed of off-the-shelf components.

Since one of the most important factors for obtaining a good, high contrast image is to collect enough photons, it is evident that good optics for optimal collection of light is necessary. These optical performance requirements for the microscope will be discussed in detail. In this design, the MEMS mirror acts as limiting system aperture and directly translates into the amount of laser beam clipping for a given beam diameter. Gaussian beam formulas are valid for an aperture-to-beam-radius $T > 1.6$. The beam diameter on the other hand translates to necessary relay optics for an addressed Numerical Aperture ≥ 0.4. On the demonstration setup these different figures of merit are discussed and compared with first images taken of biological samples.

1. Introduction

Fluorescence confocal laser scanning microscopy (F-LSM) was invented by Minsky in 1957 and is now a widely used and powerful imaging technique in fundamental biological and medical research. In contrast to optical wide-field microscopes, confocal fluorescence microscopes offer several advantages. They allow performing depth resolved fluorescence imaging of 'thick' specimens with an increased imaging contrast by effectively suppressing out of focus light. Due to this ability to selectively survey cross-sections of skin in a non-invasive manner F-LSM has been proven to be a promising tool in dermatologic diagnostics by Lademann et al. [1,2]. With this imaging technique it is possible to qualitatively evaluate dynamic skin processes and to perform penetration and distribution studies of topically applied substances in vivo and instantaneously. The only preparation needed for these measurements is the upfront application of a fluorescent contrast agent to label the skin structure. Here, fluorescein is one of the most prominent, nontoxic and FDA approved fluorescent dye, which has been used in the above cited studies. However, despite these benefits which can lead to a reduction of performed biopsies, this technique is so far uncommon in medical praxis. Factors which impede the establishment are high cost and large outlines of the F-LSM systems dealt with in medical and biological research. In dermatologic diagnostics it would be desirable to a have a space saving, moderately prized system with a large field of view and a resolution appropriate for cell imaging. To achieve miniaturization of F-LSMs several approaches have been pursued within the last 10 years. Among them fibre scanning endoscopes are prominent examples [3–7]. These endoscopes are designed for in vivo imaging inside the human body and possess in consequence a restricted field of view. However, in dermatology a large field of view is of high interest. It is for this reason, that we designed a robust and portable MEMS-based laser scanning fluorescence microscope. A few F-LSMs based on dual axis MEMS scanners have been reported in the past, but these systems are still objects of research and their field of few is smaller [8–14]. With the applied dual axis MEMS mirror (Fraunhofer IPMS) in our alternative design a larger field of view is possible. This design presented here is a demonstration system to show the possibility to build up an affordable microscope and to prove its functionalities. To keep the total cost for the components down (<40,000 USD with the laser source

* Corresponding author. Tel.: +49 351 8823 438; fax: +49 351 8823 266.
E-mail addresses: christin.bechtel@ipms.fraunhofer.de (C. Bechtel), jens.knobbe@ipms.fraunhofer.de (J. Knobbe), heinrich.grueger@ipms.fraunhofer.de (H. Grüger), hubert.lakner@ipms.fraunhofer.de (H. Lakner).
[1] Tel.: +49 351 8823 270.
[2] Tel.: +49 351 8823 155.
[3] Tel.: +49 351 8823 111.

0030-4026/$ – see front matter © 2013 Elsevier GmbH. All rights reserved.
http://dx.doi.org/10.1016/j.ijleo.2013.07.091

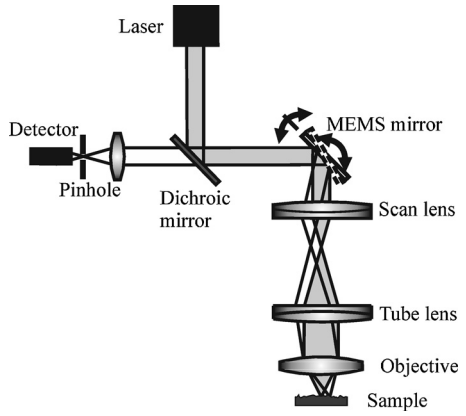

Fig. 1. Schematic optical train of the confocal laser scanning fluorescence microscope based on a dual axis MEMS mirror (Fraunhofer IPMS).

included, compared to more than a hundred thousand USD for an ordinary LSM) this F-LSM is mainly composed of off-the-shelf components. Here, a further reduction in size and the transformation into a handheld system is possible. Challenges and implications associated with the integration of a dual axis MEMS mirror will be outlined. Besides the requirements on the MEMS scanner as there is for example the θD-product [15] which directly translates to the maximum number of resolvable spots [16], the integration of this mirror is accompanied by a number of further requirements on the optical elements included in the design. Thus the choice of a MEMS mirror considerably affects the overall system layout.

Important figures of merit for the system performance, as there is the lateral and axial resolution as well as the number of fluorescence photons reaching the detector will be discussed and set into relation with the chosen components. Furthermore we will analyze the associated wave front aberrations and their impact on the performance in detail. The optimization of the overall system is performed with commercially available optical design software. To demonstrate the predicted performance and the applicability to image biological samples we demonstrate first images taken with a demonstration system. In the summary we will give an idea of future prospects.

2. System overview

The microscope is based on a dual axis MEMS mirror where the confocal character resides in the use of the same path for illumination and detection, and in the spatial filtering of the signal collected from the specimen plane. The optical train of the microscope is illustrated in Fig. 1. For illumination a laser of 488 nm wavelength is used in the design process, since this wavelength is typically used for fluorescein excitation. The laser light is coupled into a single mode fibre and subsequently collimated by a collimator at the distal end. With a dual axis MEMS mirror the beam is than deflected angularly in two directions and afterwards expanded by means of a telescope. This intermediate relay optics, consisting of a scan lens and tube lens, expands the laser beam and images the scan mirror in the entrance pupil of the microscope objective. Based on the angular movement of the beam filling the entrance pupil a lateral movement of the focus across the focal plane is achieved. A fraction of the light emitted by excited fluorophores is collected by the objective lens and descanned along the original illumination path. Finally the fluorescence light is separated from the excitation light by a dichroic mirror before being focussed onto a pinhole. For detection an avalanche photodiode is placed behind the pinhole and the image is reconstructed by correlating the measured intensity and the position information.

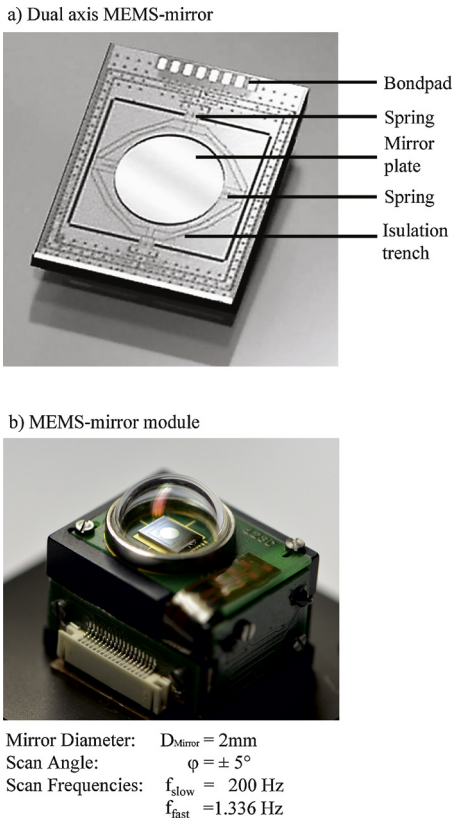

Fig. 2. (a) Photograph of a resonantly driven dual axis MEMS mirror and (b) photograph of a mounted MEMS mirror module with integrated electronic interface.

3. Design considerations

3.1. MEMS mirror

In our design, a resonantly driven dual axis MEMS mirror (Fig. 2) is employed which features a mirror size D of 2 mm diameter while maintaining fast scanning speed at resonant frequencies of 200 Hz and 1.336 kHz at the slow and fast axis, respectively. Together with a maximum scan angle φ of $\pm 5^\circ$ a Lissajous pattern is scanned. In combination with the collimated beam diameter these specifications have great impact on the total illumination time per pixel and the maximum number of resolvable spots. The determining factor for the appearance of changes in the Gaussian laser beam is the ratio of the aperture-to-beam-radius $T = r_{eff}/r_0$. Changes in the characteristics even occur for weak diffraction in the far field for an aperture-to-beam-radius in the range of [17]

$$1.6 < \frac{r_{eff}}{r_0} < 3. \quad (1)$$

Here r_{eff} is denoting the aperture radius and r_0 is the $1/e^2$ intensity beam radius in the aperture plane [17]. In these cases the beam still looks like a Gaussian beam in the far field with side lobes appearing. Considering, that due to geometrical constraints the minimum angle enclosed by the incoming light beam and the surface normal of the mirror is $\alpha = 30^\circ$, the effective mirror diameter and thus the aperture decreases as a cosine function to

$$D_{eff} = \cos(30^\circ).D = 1.73\,\text{mm} \quad (2)$$

To ensure Gaussian illumination and to minimize the following relay optic, which will be discussed later on, we decided on

a beam diameter of 1.1 mm. This is equivalent to an aperture-to-beam-radius of

$$T = \frac{r_{\text{eff}}}{r_0} = 1.6 \tag{3}$$

The number N_θ of resolvable spots for the scanner is given by the ratio of the total optical scan angle θ, which is twice the total mirror scan angle of 2φ, and the smallest resolvable spot size given by

$$\Delta\varphi = k \cdot \lambda \cdot \frac{1}{D_{\text{eff}}}. \tag{4}$$

Here k is denoting the aperture shape factor which is equal to $\pi/4$. Thus, the total number N_θ of resolvable spots is proportional to the θD-product [15] for the mirror and inversely proportional to the light wavelength $\lambda_{\text{em}} = 520$ nm and the aperture shape factor k:

$$N_\theta = \frac{\theta \cdot D_{\text{eff}}}{k \cdot \lambda} \approx 990 \tag{5}$$

Directly correlated to the number N_θ of resolvable spots is the pixel dwell time. For a sinusoidal motion of the resonant MEMS mirror, the pixel illumination time at the centre of the scan is given by [18]

$$t = \frac{1}{\pi \cdot f_{\text{fast}} \cdot N_\theta} = 2.4 \times 10^{-7}\,\text{s}, \tag{6}$$

with f_{fast} denoting the fast axis scanning frequency of 1336 Hz. As will be seen later on this pixel dwell time has a great impact on the number of photons available for detection.

3.2. The objective

The microscope objective focuses the illumination beam into the fluorescent specimen, collects a fraction of the emitted fluorescence light and directs it back to the scanning unit. An important optical property of microscope objectives for fluorescence applications is the Numerical Aperture (NA) which determines the resolution limit of a diffraction limited optical system for a given wavelength. Additionally a large NA enables the objective to collect a higher fraction of the light emitted by the fluorescence specimen. Besides the NA further important requirements in the field of biological applications involving 3D measurement are a reasonable working distance, chromatic correction and high transmission. Especially the colour correction is crucial due to the difference in excitation and emission wavelength of fluorescence specimen. Considering these requirements we decided on a CFI Plan Apochromat VC 20 × 0.75 (Nikon, Japan) with a focal length $f = 10$ mm and a working distance of 1 mm. The achievable NA of 0.75 of the objective is larger than the addressed NA of 0.4, which is adequate for performing 3D sectioning. With a NA of 0.4 the resulting spot radius ω_o and a Rayleigh range z_R are

$$\varpi_0 = 0.5 \cdot k \cdot \lambda_{\text{ex}} \cdot f/\# = 0.49\ \mu\text{m} \tag{7}$$

$$z_R = \frac{\pi}{\lambda_{\text{ex}}} \cdot (\varpi_0)^2 = 1.54\ \mu\text{m}. \tag{8}$$

To achieve the latter, the laser beam entering the objective needs to have a diameter of

$$D = 2 \cdot \text{NA} \cdot f = 7\,\text{mm}, \tag{9}$$

which results effectively in an under filling of the objective pupil. As a consequence, the intermediate optics has to provide a beam expansion ratio of at least 6.4 to expand the illumination beam from a diameter of 1.1 mm to 7 mm. With a magnification of $M = 7$ the field of view is given to have a diameter of

$$d_{\text{im}} = 2 \cdot f \cdot \tan\left(2 \cdot \frac{\varphi}{M}\right) = 500\,\mu\text{m}, \tag{10}$$

where φ denotes the mirror scan angle of 5°.

3.3. The intermediate optics

Upon investigating the requirements on the objective and the mirror the role of the intermediate optic is to expand the beam diameter up to at least 7 mm while maintaining the telecentric properties by forming an image of the mirror in the entrance pupil of the objective. To realize the magnification a telecentric system arranged as a keplerian telescope is used. According to this telescope principle, the required magnification of $M = 7$ results from the ratio of the focal lengths of the scan lens f_{scan} located close to the scanning mirror and the tube lens f_{tube} next to the objective:

$$M = \frac{f_{\text{tube}}}{f_{\text{scan}}} = 7. \tag{11}$$

For both lenses commercially available components where applied to ensure a cost effective system. Since the setup is aimed for employing fluorescence measurements in biological tissue, they are chosen to be achromates to avoid dispersion effects for the excitation and emission wavelength. An additional advantage is that achromates are known to have less spherical aberration. Taking these factors and the scanning angle of ±5° into consideration the application of a hasting triplet with 20 mm focal length as scan lens and an achromat with 140 mm focal length as tube lens is favourable. With a relatively short focal length of 20 mm the scan lens not only provides enough space for mounting but also minimizes the optical path throughout the intermediate optics.

3.4. Pinhole

In a confocal microscope out-of-focus light is prevented from reaching the detector by a pinhole mounted in a conjugate focal plane to the specimen plane. Hereby the detection is limited to emission occurring near the focal spot and does not only provide in depth discrimination but also optimizes the image contrast by suppressing stray light. Lateral and axial discrimination is managed because out-of-focus light in axial direction will be focused either in front or behind the pinhole and out-of-focus light in the focal plane will miss the pinhole in lateral direction. The size of the pinhole is usually set to be equal to a diameter of 0.7–1.5 Airy Units corresponding to a diffraction limited spot on the plane of the pinhole [19]. With a given magnification M of the relay system and a lens of 40 mm focal length for focussing the fluorescence light onto the pinhole, the NA at the pinhole is given by

$$\text{NA}_{\text{pin}} = \frac{\text{NA}_{\text{Obj}} \cdot f_{\text{Obj}}}{M \cdot f_{\text{pin}}} = 0.014 \tag{12}$$

and yields an Airy Unit (AU) of

$$D_{\text{Airy}} = \frac{1.22 \cdot \lambda_{\text{em}}}{\text{NA}_{\text{pin}}} = 48\,\mu\text{m} \tag{13}$$

for a maximum fluorescence emission spectra around 520 nm. Here, the NA_{Obj} is 0.4 and not the achievable NA of 0.75 of the objective. This is due to the fact that the MEMS mirror acts as the limiting aperture. Thus, choosing a pinhole of 50 μm diameter, relates to a diameter of 1.04 AU and a throughput of around 80% of the light in the central maximum [20].

3.5. Illumination requirements

The amount of laser power needed depends crucially on the chosen fluorescence specimen being studied. Fluorescent dyes are characterized by both biochemical and spectroscopic properties. The latter primarily determines the number and energy distribution of photons available for detection and allows an estimation of how many photons can be tolerated per pixel before saturation of the fluorescence dye takes place. Using a 488 nm laser we decided among the suitable Fluorophores on AlxaFluor 488 from Molecular Probes (Invitrogen, Carlsbad, CA) due to its good spectral properties. Outstanding characteristics of AlexaFluor 488 dyes are their low sensitivity on environmental factors such as pH, aqueous exposure and dye–dye interactions resulting directly or indirectly to improved photo stability [19,21,22]. Additionally AlexaFluor 488 exhibits a short lifetime of 4.1 ns [22] leading to a maximum emission rate F

$$F = \frac{1}{\tau} = 2.44 \times 10^8 \text{ Photons/s} \tag{14}$$

emitted and absorbed photons per second. In spite of this relatively short lifetime, which is comparable to fluorescein, the minimum pixel dwell time of 0.24 μs in the centre of the field limits the emission rate to a 58 detectable photons per dye molecule and pixel. In combination with the remaining dye specific characteristics as there is the molecular cross section σ of 2.79×10^{-16} cm^2 and the Quantum Yield (QY) of 0.92, the maximum excitation photon flux I before saturation is

$$I = \frac{F}{\sigma \cdot QY} = 9.50 \times 10^{23} \text{ Photons/cm}^2\,\text{s} \tag{15}$$

In combination with the lateral resolution, illuminated volume and dye concentration the necessary laser power before saturation takes place and the number of emitted photons can be estimated. As mentioned earlier lateral and axial illumination parameters are dependent on the aperture to beam radius which defines the truncation ratio of the laser beam. Thus the illuminated volume in the sample is given by

$$V = \frac{4}{3} \cdot \pi \cdot r_{\text{lat}}^2 \cdot r_{\text{axial}} \tag{16}$$

with an $1/e^2$ intensity beam radius of

$$\omega_0 = 0.5 \cdot k \cdot \lambda_{\text{ex}} \cdot f/\# = 0.49\ \mu\text{m} \tag{17}$$

in lateral direction and with the Rayleigh range in axial direction

$$z_{\text{R}} = \pm \frac{\pi}{\lambda_{\text{ex}}} \cdot \varpi_0^2 = 1.54\,\mu\text{m}. \tag{18}$$

Accordingly the number of dye molecules within the spot of focus is given by

$$N_{\text{dye}} = V \cdot c_{\text{dye}} \cdot N_{\text{A}} = 9330 \tag{19}$$

for an assumed dye concentration of $c_{\text{dye}} = 10$ μmol/l and N_{A} denoting the Avogadro constant. With a maximum scan time per pixel of $t_{\text{scan}} = 0.24$ μs this leads to a minimal number of emitted photons given by

$$N_{\text{Photon}} = N_{\text{dye}} \cdot F \cdot t_{\text{scan}} = 5.46 \times 10^5 \tag{20}$$

per pixel. The necessary laser power to realize the above stated photon flux for maximum fluorescence emission is given by:

$$P_{\text{Laser}} = I_{\text{max}} \cdot E_{\text{Photon}} \cdot \pi \cdot r_{\text{lat}}^2 = 5.5\,\text{mW} \tag{21}$$

Such intensities excite fluorophores so rapidly that no molecules are left in the ground state and the emission rate will be limited by the excited-state lifetime. Hence the emission is saturated and a further increase of the intensity will not lead to a significantly higher output. However, only a small percentage of the emitted photons reach the detection path since the radiation occurs in all directions and even less photons are finally available for detection. With a NA of 0.4 only photons emitted within the solid angle of

$$\Omega = 2\pi \cdot \left(1 - \cos\frac{\alpha}{2}\right) \tag{22}$$

where α denotes the apex angle

$$\alpha = 2 \cdot \sin^{-1}(\text{NA}) = 23^\circ \tag{23}$$

can enter the objective. This corresponds to a photon loss of

$$1 - \frac{\Omega}{\Omega_{\text{total}}} = 1 - \frac{1 - \cos(\alpha/2)}{2 \cdot \pi} = 96.1\% \tag{24}$$

which corresponds to 21,300 photons that reach the detection path. Thus, it is crucial for the overall performance that the optical system is highly corrected to prevent further losses.

Table 1
Estimated losses of the initial number of photons emitted by the fluorescence sample in the detection path.

Element	Loss (%)	Remainder (%)
Sample emission		100
Collection by effective NA of 0.4	96.1	3.9
Relay optic	10	3.5
MEMS mirror	15	3.0
Dichroic mirror	5	2.8
Filter	20	2.3
Pinhole	20	1.8
Percentage of emitted photons reaching the detector		1.8

3.6. Detection unit

For detection only the fraction of emitted fluorescence light is available which is collected by the objective, descanned along the original illumination path and finally separated from the excitation light by a dichroic mirror. Further elimination of the excitation light in front of the pinhole and the detector is achieved by additional filters. As the total number of photons reaching the detector is an important selection criterion of the latter, an estimation of the fraction of photons passing the optical system suggests itself. Assuming intensity losses as shown in Table 1, only 1.8% of the emitted photons are available for detection, which is equivalent to 9900 photons per pixel. Additional criteria are the bandwidth and the signal to noise ratio of the photodiode and its amplifier.

3.7. Z-shifter

For the acquisition of a three-dimensional image of the fluorescence specimen, it has to be scanned in three directions. There are in principle two solutions for moving the beam while keeping the object stationary, an axial movement of the objective lens or a movement of the focus by the intermediate optics [23]. Whereas the latter can be ruled out, since a change in the focus position by movements of the intermediate optics would require by far too large movement distances since the axial magnification M_z is the square of the lateral magnification M:

$$M_z = M^2 \tag{25}$$

Thus a focus shift of 10 μm in object plane would lead in our case, with a lateral magnification of $M = 7$ to a focus shift of

$$\Delta z_{\text{int}} = \Delta z_{\text{Obj}} \cdot M^2 = 4.9\ \text{mm} \tag{26}$$

in the intermediate image plane. Hence the method of choice is to use a piezoelectric z-shifter to move the objective. This arrangement ensures an excellent, backlash-free operation over a range of 100 μm with a position repeatability in z-direction of ±10 nm.

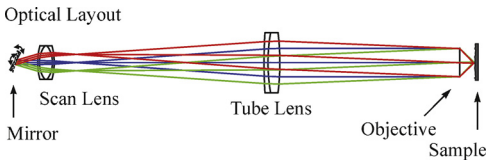

Fig. 3. Optical layout with rays traced for three different elongations of the dual axis MEMS mirror. The objective is modelled as an ideal lens.

4. Optical design

In the design process several constraints, such as minimal space requirement and the utilization of commercially available components, were applied to the problem so as to develop a portable and cost effective scanning microscope with an appropriate performance for biological applications. In order to achieve an optimal arrangement, a simulation of the optical setup by means of commercially available optical design software was performed. In the design and analysis of the optical system, rays were traced forward from infinity at the mirror plane through the intermediate optic to the exit pupil of the objective for different field angles and wavelengths. Since microscope objectives are usually very well corrected lenses, the objective is modelled as an ideal lens with 10 mm focal length. The wavelengths were chosen according to the laser and the fluorescence emission wavelength at 488 nm and 520 nm, respectively. The optical design layout is depicted in Fig. 3.

In the final optimization and analysis stages, the Strehl ratio was used as a figure of merit. According to the Rayleigh criterion a diffraction limited performance is given for a Strehl number larger than 0.8 which corresponds to a peak-to-valley value of the wave aberration smaller than $\lambda/4$ [24]. As shown in Fig. 4b a nearly diffraction limited performance is given over the full field. In addition the corresponding Point Spread Function (PSF) in Fig. 4a shows that for the maximum angle of 10° the spot size is around 1.2 μm. This demonstrates the capability of the system to image cell nuclei with a diameter of 6 μm. For cell imaging in biology this optical arrangement is an adequate tool. To more closely examine the kind of aberrations present in the system the Optical Path Difference (OPD) is plotted in Fig. 5a for the different field angles. It is obvious that for larger field angles coma is the dominant aberration in this geometry. The main reason is the remote stop position given by the arrangement of the MEMS mirror in front of the scan lens. This eliminates the symmetry of the optical system about the principal ray which would help to reduce coma, distortion and lateral colour. By the fact that the chosen Hasting Triplet is aimed for achromatic applications it is designed with focus on the reduction of "pincushion" distortion, lateral colour and spherical aberration. Unfortunately simultaneous correction of coma and spherical aberration is not possible in this case when a reasonably flat field is demanded. Thus we have to deal with a higher amount of coma due to the correction of spherical aberration. Albeit in our case the correction of spherical aberration would not have been necessary to this extend. The reason is the relatively small beam diameter in comparison to the focal length of the scan lens which already tends to hold spherical aberration to a reasonable value.

Another characteristic of the system important to look at is the field curvature because of the relatively short focal length of the scan lens. Nevertheless, this system possesses a moderate field curvature with 1.8 μm (as illustrated in Fig. 5b) which does not affect the image quality considerably due to the effect of the pinhole. The pinhole rejects out-of-focus light and automatically

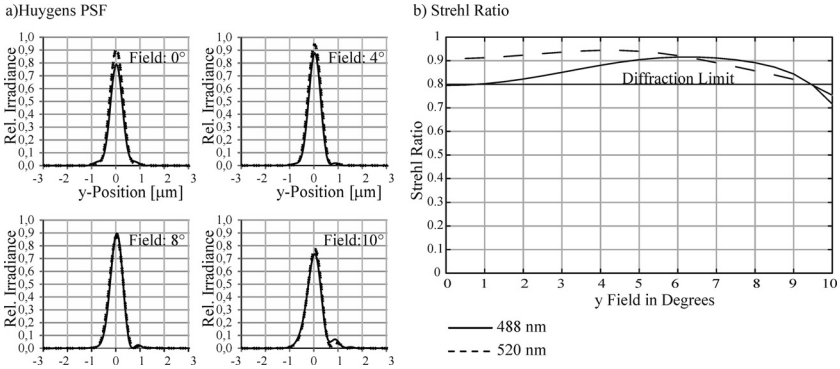

Fig. 4. Predicted performance of the optical design in Fig. 3. (a) Huygens PSF for four different field angles and (b) Strehl ratio as a function of the field angle.

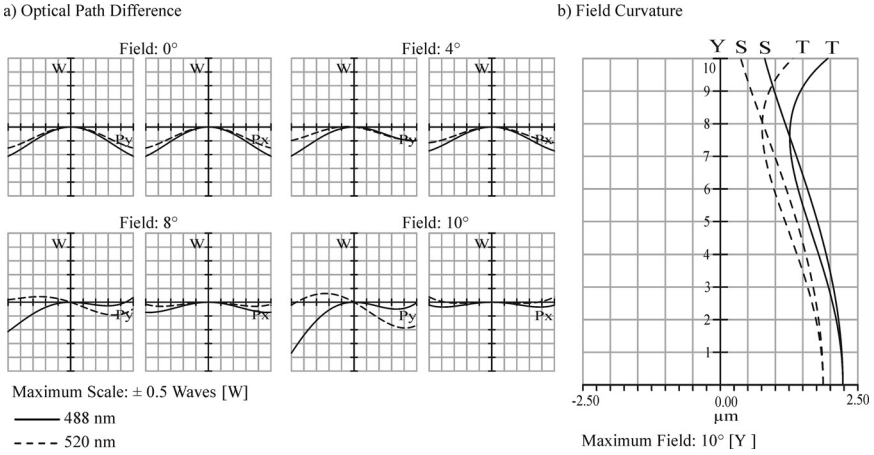

Fig. 5. (a) Wave aberration at the exit pupil of the objective for four different field angles. (b) Field curvature in tangential and sagittal direction.

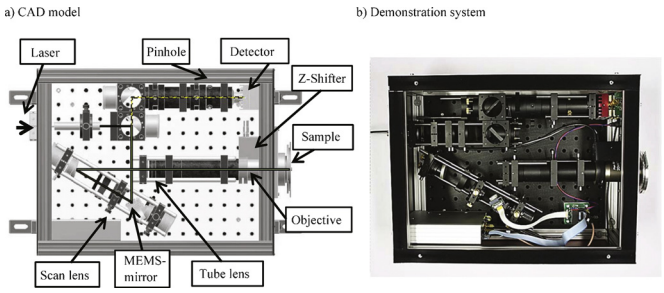

Fig. 6. (a) Computer-aided-design and (b) Photograph of a MEMS-based confocal laser scanning fluorescence microscope demonstration system.

image the surface of best focus. Especially in the case of biological probes, the sample preparation already influences the position and elongation to a much greater extent. Hence aberrations such as defocus and field curvature are nearly eliminated.

In total these aberrations restrict the maximum scanning angle to $\pm 10^{\circ}$. The maximum spot size for a field angle of 10° is around 1.2 μm in diameter. In conclusion this design is expected to show an adequate performance over the whole field of view of 0.5 mm in diameter for the addressed application of cell imaging.

5. Experimental setup

To verify these results a demonstration setup (340 mm × 240 mm × 15 mm) has been build and first test measurements were made. In Fig. 6, a CAD model and the final demonstration system is depicted. The principle setup is depicted in Fig. 7 and consists of a laptop, a remotely connected power and control unit and the microscope system with an integrated electronics module. A USAF1951 resolution test target was placed on top of a FluoRef™ fluorescence reference slide and imaged to prove the resolving power of the microscope (Fig. 8b). These fluorescence slides are made of plastic and provide a continuous fluorescent field. In this sample the smallest element in group 7 has 228 line pairs/mm, corresponding to a line width of 2.2 μm. The conical distortion present in this image is a well-known artefact originating from the angle of the incoming laser beam to the surface normal of the MEMS mirror [25]. This distortion can be corrected by post processing.

In Figs. 8a and 9 'thick' biological samples of fluorescent stained convalaria are imaged. As can be easily seen only one layer of cells is imaged. The depth difference of the images in Fig. 9 are 3 μm and hence an in depth discrimination is obvious. These first images are promising and indicate that the resolution is indeed sufficient for cell imaging.

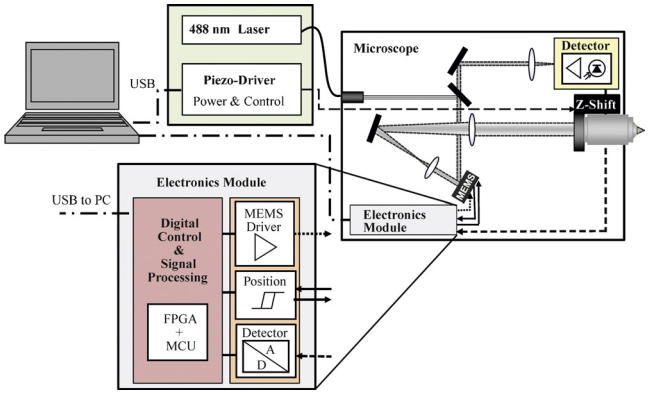

Fig. 7. Principle setup: laptop, remotely connected power and control unit, and the microscope system with an integrated electronics module.

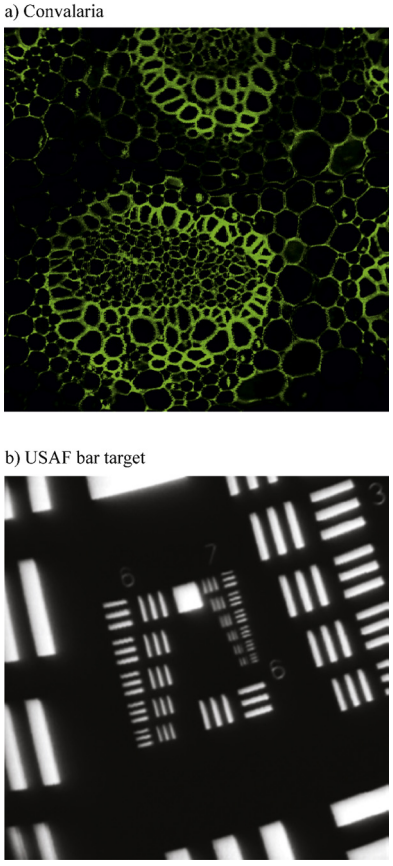

Fig. 8. (a) Fluorescent image of Convalaria (Lily of the Valley) and (b) Fluorescence image of a USAF1951 target obtained with the demonstration setup of the confocal laser scanning fluorescence microscope.

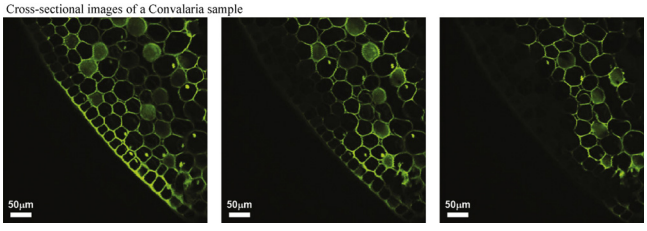

Fig. 9. Cross-sectional images of a Convalaria sample with depth differences of 3 μm.

6. Summary and conclusion

Confocal fluorescence laser scanning microscopes are well established and widely used in biological and medical research. Their capability to selectively survey cross-sections of individual layers from 'thick' samples makes them a promising tool in dermatologic diagnostics as well. However, due to their main application area in research, these instruments dealt with here are either complex laboratory systems which are stationary and accordingly cost-intensive or they are endoscopes exhibiting a small field of view. It is for this reason we have developed a robust and portable MEMS-based confocal laser scanning fluorescence microscope composed of off-the-shelf components with a field of view of 500 μm × 500 μm. We demonstrated the interrelations of the optical components for the presented design and discussed their impact on the photon loss in the detection path as well as the overall performance. With more detailed analysis by means of optical simulations and first test measurements with a demonstration

setup the system has been characterized and found to meet the requirements for cell based fluorescence measurements. First measurements have shown a lateral and axial resolution of 2.2 μm and 3 μm, respectively with a field of view of 500 μm × 500 μm. Thus, we have shown the possibility to realize a robust and affordable confocal laser scanning fluorescence microscope with off-the-shelf components. The next step will be to transfer this demonstration setup to a handheld microscope system.

Acknowledgment

This research project was developed in cooperation with Fraunhofer IPMS and supported by the European Social Fund, ESF. We would like to thank Prof. Dr. Guenter Huber (Institute of Laser Physics, Hamburg University) for providing the frequency doubled OPS laser (λ = 480 nm) which was used as an excitation source in this work.

References

[1] L.E. Meyer, J. Lademann, Application of laser spectroscopic methods for in vivo diagnostics in dermatology, Laser Phys. Lett. 4 (2007) 754–760.
[2] J. Lademann, N. Otberg, H. Richter, L. Meyer, H. Audring, A. Teichmann, S. Thomas, A. Knüttel, W. Sterry, Application of optical non-invasive methods in skin physiology: a comparison of laser scanning microscopy and optical coherent tomography with histological analysis, Skin Res. Technol. 13 (2) (2007) 119–132.
[3] F. Helmchen, M.S. Fee, D.W. Tank, W. Denk, A miniature head-mounted two-photon microscope: high-resolution brain imaging in freely moving animals, Neuron 31 (6) (2001) 903–912.
[4] H. Bao, J. Allen, R. Pattie, R. Vance, M. Gu, Fast handheld two-photon fluorescence microendoscope with a 475 μm × 475 μm field of view for in vivo imaging, Opt. Lett. 33 (12) (2008) 1333–1335.
[5] C.J. Engelbrecht, R.S. Johnston, E.J. Seibel, F. Helmchen, Ultra-compact fiber-optic two-photon microscope for functional fluorescence imaging in vivo, Opt. Express 16 (8) (2008) 5556–5564.
[6] R. Le Harzic, M. Weinigel, I. Riemann, K. König, B. Messerschmidt, Nonlinear optical endoscope based on a compact two axes piezo scanner and a miniature objective lens, Opt. Express 16 (2008) 20588–20596.
[7] J. Sawinski, W. Denk, Miniature random-access fiber scanner for in vivo multiphoton imaging, Appl. Phys. 102 (2007).
[8] C. Arrasmith, D. Dickensheets, A. Mahadevan-Jansen, MEMS-based handheld confocal microscope for in-vivo skin imaging, Opt. Express 18 (4) (2010) 3805–3819.
[9] H. Ra, W. Piyawattanametha, M.J. Mandella, P. Hsiung, J. Hardy, T.T. Wang, C.H. Contag, G.S. Kino, O. Solgaard, Three-dimensional in vivo imaging by a handheld dual axes confocal microscope, Opt. Express 16 (10) (2008) 7224–7232.
[10] L. Fu, A. Jain, H. Xie, C. Cranfield, M. Gu, Nonlinear optical endoscopy based on a double-clad photonic crystal fiber and a MEMS mirror, Opt. Express 14 (3) (2006) 1027–1032.
[11] T.M. Liu, M.C. Chan, I.H. Chen, S.H. Chia, C.K. Sun, Miniaturized multiphoton microscope with a 24 Hz frame-rate, Opt. Express 16 (14) (2008) 10501–10506.
[12] W. Jung, S. Tang, D.T. McCormic, T. Xie, Y.C. Ahn, J. Su, I.V. Tomov, T.B. Krasieva, B.J. Tromberg, Z. Chen, Miniaturized probe based on a microelectromechanical system mirror for multiphoton microscopy, Opt. Lett. 33 (12) (2008) 1324–1326.
[13] W. Piyawattanametha, E.D. Cocker, L.D. Burns, R.P.J. Barretto, J.C. Jung, H. Ra, O. Solgaard, M.J. Schnitzer, In vivo brain imaging using a portable 2.9 g two-photon microscope based on a microelectromechanical systems scanning mirror, Opt. Lett. 34 (15) (2008) 2309–2311.
[14] J.T.C. Liu, M.J. Mandella, N.O. Loewke, H. Haeberle, H. Ra, W. Piyawattanametha, O. Solgaard, G.S. Kino, C.H. Contag, Micromirror-scanned dual-axis confocal microscope utilizing a gradient-index relay lens for image guidance during brain surgery, J. Biomed. Opt. 15 (2) (2010).
[15] L. Beiser, Laser scanning systems, in: M. Ross (Ed.), Laser Applications, Academic Press, New York, 1974, pp. 55–159.
[16] H. Urey, D.W. Wine, T.D. Osborn, Optical performance requirements for MEMS-scanner based microdisplays, Proc. SPIE 4178 (2000) 176–185.
[17] P. Belland, J.P. Crenn, Changes in the characteristics of a Gaussian beam weakly diffracted by a circular aperture, Appl. Opt. 21 (3) (1986).
[18] H. Urey, N. Nestorovic, B. Ng, A. Gross, Optics designs and system MTF for laser scanning displays, Proc. SPIE 3689 (1999) 238–248.
[19] I.D. Johnson, Practical Considerations in the Selection and Application of Fluorescent Probes, Handbook of Biological Confocal Microscopy, Springer, J.B. Pawley, 2006, pp. 353–367.
[20] M. Born, E. Wolf, Principles of Optics, Cambridge University Press, 1999.
[21] J.R. Lakowicz, Priciples of Fluorescence Spectroscopy, Springer Press, 2010.
[22] R.P. Haugland, Molecular Probes Handbook: A Guide to Fluorescent Probes and Labeling Technologies, Life Technologies, 2010.
[23] E.H.K. Stelzer, The intermediate optical system of laser-scanning confocal microscopes, in: J.B. Pawley (Ed.), Handbook of Biological Confocal Microscopy, Springer, 2006, pp. 207–220 (Chapter 9).
[24] H. Gross, H. Zugge, M. Peschka, F. Blechinger, Handbook of Optical Systems, Wiley, Weihnheim, 2005.
[25] M. Scholles, K. Frommhagen, C. Gerwig, J. Knobbe, H. Lakner, D. Schlebusch, M. Schwarzenberg, U. Vogel, Recent advancements in system design for miniaturized MEMS-based laser projectors, Proc. SPIE 6911 (2008).